



Cite this: *J. Anal. At. Spectrom.*, 2025, **40**, 2487

Single particle inductively coupled plasma mass spectrometry for the characterization of colloidal particles in soils, sediments and sludges: comparative study of sector field and time-of-flight instruments

Zhizhong Li, Madjid Hadioui  and Kevin J. Wilkinson *

Colloids and nanoparticles in solid phase environmental matrices (soils, sediments, sludges) are widely heterogeneous and polydisperse, which complicates their sampling and characterization by bulk analysis techniques. Indeed, techniques based upon single particle measurements are better equipped for identifying important, but low frequency, properties or characteristics which are needed to understand the function of environmental colloids. In this study, a continuous flow extraction assisted by ultrasound was used to sample colloidal particles from several solid matrices. The high sensitivity of a sector field ICP-MS and the quasi-instantaneous, multi-isotope measurements of a time-of-flight ICP-MS were combined to enable the characterization of colloidal particles extracted from soils, sediments and sludges. Single particle (SP) analysis of the particle leachates using the sector field instrument (SP-ICP-SF-MS) led to the detection of larger numbers (up to 6800×) of Mg-, Al-, Si-, Ca-, Ti-, Fe-, and Ba-containing particles than measured by single particle time-of-flight ICP-MS (SP-ICP-ToF-MS), largely due to the different size detection limits of the techniques, *i.e.* ca. 16 nm by SP-ICP-SF-MS and 76 nm by SP-ICP-ToF-MS, when measuring aluminosilicates. Despite the limitation of SP-ICP-ToF-MS in detecting smaller particles, the technique was successfully used to identify mineral phases of illite, vermiculite, and smectite based on elemental ratios in the individual particles. The multi-isotope capability of the SP-ICP-ToF-MS was also used for the determination of isotopic ratios in both individual particles and bulk digested leachates. Mean $^{206}\text{Pb}/^{207}\text{Pb}$ ratios in the particles extracted from the solid phase samples deviated from measurements obtained from bulk digestions by 1.2–5.9%, indicating the potential of the SP-ICP-ToF-MS to perform such measurements. SP-ICP-SF-MS and SP-ICP-ToF-MS were complementary for obtaining insight into the composition and particle size distributions of the colloids and nanoparticles. Specifically, neither technique gave the complete particle size distribution due to their complementary size detection windows.

Received 4th May 2025
 Accepted 1st August 2025

DOI: 10.1039/d5ja00181a

rsc.li/jaas

1. Introduction

Nanoparticles (NP) and colloidal particles (CP) are omnipresent in the environment, arising from both natural processes and anthropogenic activities. In soils, these particles play an important role in the mobilization of both nutrients and contaminants.¹ Furthermore, particle size is recognized as a key factor governing particle fate and behavior, with the smallest particles playing a key role in particle mobility and bioavailability.² In soils and sediments, particles are polydisperse^{3,4} and while the smallest particles might contribute minimally to overall particle mass, their contribution to environmental

function and ecological risk can be important if they are enriched in components with high suspected toxicity (*e.g.* As, Pb, Cd). In that context, bulk measurement techniques are useful for providing information on the overall (average) composition of a bulk sample, but they cannot distinguish individual particle types (*e.g.* 1 pure Fe particle in 100 cannot be distinguished from a population of particles containing 1% Fe). Furthermore, a single 1 μm particle will have the same mass as 10⁶ NP (10 nm), but arguably a very different environmental risk. For these reasons, single particle techniques, providing both particle size distributions and single particle compositions should be able to provide much better insight into the function and risk associated with solid phase environmental particles.

Single particle inductively coupled plasma mass spectrometry (SP ICP-MS) is a relatively new technique that allows for the analysis of metallic constituents within nanoparticles and

Biophysical Environmental Chemistry Group, Department of Chemistry, University of Montreal, 1375 Ave. Thérèse-Lavoie-Roux, Montreal, H2V 0B3, Canada. E-mail: kj.wilkinson@umontreal.ca; Fax: +1-514-343-7586; Tel: +1-514-343-6741



colloids^{5–9} on a particle-by-particle basis. Quadrupole and magnetic sector based ICP-MS are typically limited to measuring one or two elements per particle, complicating the analysis of chemical complex solid phase particles. While a multi-collector ICP-MS (MC ICP-MS) can allow for the simultaneous measurement of multiple elements, it is contingent upon prior knowledge of the specific elements present.^{10–13} Single particle inductively coupled plasma time-of-flight mass spectrometry (SP-ICP-ToF-MS) has the capacity to provide comprehensive analysis without the need for pre-defined elements, making it a powerful tool for the detection and characterization of natural colloids and nanoparticles.^{14–20} SP-ICP-ToF-MS can measure most elements in small particles (~30 nm–2 μm) concurrently, allowing for the measurement of elemental and isotopic ratios of individual NP and CP. In spite of the obvious advantages of the SP-ICP-MS techniques, there are several difficulties associated with the measurement of chemically heterogeneous and polydisperse natural samples (soils, sediments, sludges) by SP-ICP-MS. For example, the composition of small particles can be difficult to distinguish from dissolved (background) metals. Furthermore, it can be difficult to distinguish small numbers of particles that are important to environmental function from the much more common major elements (*e.g.* aluminosilicates, metal oxides and phosphates).

In order to accurately characterize colloidal particles in soils, effective extraction methods are crucial. Regelink *et al.*²¹ tested a number of extracting agents to isolate nanoparticles from soil, while Baur *et al.*²² employed surfactant assisted extraction to recover nanoparticles from a road runoff sediment. Li *et al.*²³ explored the use of an ultrasound probe to batch-extract colloidal particles from soils, which favoured the extraction of large amounts of smaller particles. Other authors^{24,25} have favored batch extractions with sonic baths and different extractants in order to sample small colloidal particles from soils. In that case, Na₄P₂O₇ was found the most efficient extractant as it led to 2–12× more leached particles as compared to other extracting agents (NaOH, Na₂CO₃, Na₂C₂O₄). Schwertfeger *et al.*²⁶ studied the impact of different parameters, including the use of ultrasonic baths or probes and different extracting agents, on the recovery of engineered silver nanoparticles spiked into biosolids/soils. The combination of Na₄P₂O₇ and an ultrasonic probe led to the highest extraction efficiency.

The aim of this work was to develop a robust methodology to obtain particle-by-particle information on colloids and nanoparticles on several solid phase samples using SP-ICP-SF-MS

and SP-ICP-ToF-MS. An ultrasound-assisted, continuous-flow technique was used to extract nanoparticles and colloids from solid samples (two agricultural soils, a flood plain soil, a domestic sludge, an industrial sludge and a river sediment). The leachates from the complex samples were then analyzed by single particle analysis using the two techniques followed by advanced data treatment strategies.

2. Materials and methods

2.1 Chemicals

Ultrahigh or high purity reagents and ICP-MS standards (traceable to NIST) were used in this work. These included ultrapure nitric acid (67–70% w/w, Plasma Pure Plus, SCP-Science), trace metal grade hydrochloric acid (37% w/w, Fisher Chemical), ACS reagent grade tetrasodium pyrophosphate (Na₄P₂O₇ or TSPP, Sigma-Aldrich), single-element Au, Si and Ti ICP-MS standards (CGAU1, CGSi1 and CGTi1, Inorganic Ventures), multi-element ICP-MS standard (IV ICP-MS-71A; Inorganic Ventures), and suspensions of ultra-uniform 30, 50 and 100 nm gold nanoparticles (AUXU30-1M, AUXU50-1M and AUXU100-1M, NanoComposix). All extraction solutions and ultra-uniform gold nanoparticles were prepared using ultrapure water (Milli-Q; *R* > 18.2 MΩ cm; total organic carbon <2 μg C L⁻¹). Ionic ICP-MS standards were diluted in 1% v/v HNO₃ or 1% HCl.

2.2 Solid phase samples

Six solid phase standard reference materials (SRM 2709a, SRM 2710a, SRM 2711a, SRM 2781, SRM 2782, and SRM 8704) were purchased from the National Institute of Standards and Technology (NIST, USA). In this paper, these samples are referred to by abbreviations based upon their origin: by AG1, FP, AG2, DS, IS and RS, as detailed in Table 1. The mass fractions of some elements, based on the NIST certificate of analysis, are given in Table S1. All samples were used as received from NIST without any further pretreatment.

2.3 Ultrasound-assisted continuous-flow extraction of colloidal particles

An optimized continuous flow extraction procedure based upon the literature²¹ was used to eluate the NP and CP from the agricultural soils, sludges and river sediments. In summary, 0.5 g of dry sample (weighed to a precision of 0.1 mg) was put into a 1 mL plastic solid phase extraction cartridge

Table 1 Identification of solid phase samples used for extraction of metal containing colloidal particles

Sample ID	NIST SRM	Type/collection site
AG1	2709a	Agricultural soil, San Joaquin valley, California
FP	2710a	Flood plain, Silver Bow Creek, Montana
AG2	2711a	Agricultural soil, East Helena, Montana
DS	2781	Domestic sludge, Metropolitan Denver Sewage Disposal District No. 1
IS	2782	Industrial sludge, New Jersey
RS	8704	River sediment, Ohio Street Bridge, Buffalo



(MilliporeSigma™ Supelco™ 54220-U) with a polyethylene frit (Sigma-Aldrich) at the bottom end only. Both ends of the cartridge were tightly connected to peristaltic PVC tubing. For each experiment, triplicate columns were vertically immersed in a beaker full of water (Fig. S1). An ultrasound probe (12.7 mm titanium tip, Q500 sonicator, Qsonica L.L.C, Newtown, USA) was placed between the three columns and ultrasonication parameters were set to 250 W output amplitude using a 10 s ON and 5 s OFF pulse mode. A peristaltic pump was used to push the extraction solution through the soil from the bottom to the top of the column and then into polypropylene tubes, where extracts were collected for analysis. Based upon prior optimization experiments,²⁷ the extraction of colloidal particles was performed using 40 mM TSPP at pH adjusted to 6.0. Large particles and agglomerates were separated from the leachate by centrifugation (3000 rpm, 1882 × *g*; 5 min.; Heraeus Multifuge 1 S-R, Kendro, Germany). The collected supernatant was diluted (10³ to 10⁶×, depending on particle number) with ultrapure water prior to analysis by SP-ICP-MS.

2.4 Single particle ICP-MS analysis

SP-ICP-MS analyses were performed on two different inductively coupled plasma mass spectrometers: a double focusing magnetic sector field ICP-MS (SP-ICP-SF-MS, AttoM-ES, Nu Instruments, UK) and a time-of-flight ICP-MS (SP-ICP-ToF-MS, Vitesse, Nu Instruments, UK). Both instruments were equipped with similar sample introduction systems including a micro-flow concentric glass nebulizer (0.2- and 0.4 mL min⁻¹ for the SP-ICP-SF-MS and SP-ICP-ToF-MS, respectively), a quartz cyclonic spray chamber (Peltier-cooled to 4 °C) and a quartz injector (1.5 mm internal diameter).

SP-ICP-SF-MS measurements were performed at low resolution ($m/\Delta m = 300$), except for ²⁸Si for which data were acquired at a medium resolution of 2500. Triplicate acquisitions of 40 s were recorded using a dwell time of 40 μs for each isotope. For measurements using SP-ICP-ToF-MS, the resolution ranged from 2500 to 5800 depending on the isotope. The ICP-ToF-MS was equipped with a segmented reaction cell (SRC) to eliminate polyatomic, mainly argon and nitrogen-based, interferences.²⁸ Helium and hydrogen were continuously introduced in the SRC using flow rates that were optimized daily: in the range of 5–7 mL min⁻¹ for H₂ and 14–17 mL min⁻¹ for He. SP-ICP-ToF-MS data was acquired by recording spectra in the mass range 20–260 amu every 80 μs for a total of 5–6 minutes, depending on particle content.⁸

Instrument sensitivities were determined from an ionic calibration using single and multielement ICP-MS standards, diluted in 1% v/v HNO₃, except for Au, which was diluted 1% v/v HCl. Different concentration ranges were optimized, depending on the ICP-MS instrument and the analyte sensitivity. For SP-ICP-SF-MS, four different sets of ionic standards were prepared: (i) Si (1, 2, 5, 10, 20 and 50 μg L⁻¹), (ii) Al and Mg (0.1, 0.2, 0.5, 1, 2, and 5 μg L⁻¹), (iii) Ca, Ti, Fe and Ba (0.5, 1, 2, 5, 10 and 20 μg L⁻¹) and (iv) Au (0.02, 0.05, 0.1, 0.2, 0.5 and 1 μg L⁻¹). In the case of SP-ICP-ToF-MS, standards (0.2, 0.5, 1, 2, 5, 10, and 20 μg L⁻¹) were prepared from a 43-element standard in

addition to 2 single-element standards (Si and Ti). Transport efficiency was determined daily, and after every 20 samples, using suspensions of ultra-uniform gold nanoparticles (30 nm (50 ng L⁻¹), 50 nm (200 ng L⁻¹) and 100 nm (500 ng L⁻¹)) and ionic gold standards (0.2, 0.5, 1, 2, 5, and 10 μg L⁻¹).

Raw data were processed using manufacturer's built-in software (Nu Quant and Nu Quant Vitesse for SP-ICP-SF-MS and SP-ICP-ToF-MS data, respectively) which rely on a variable integration window (to accommodate the variation of peak widths) and smoothing (to reduce fluctuations and to facilitate accurate peak detection). Detailed descriptions can be found in the literature.^{28–30} Briefly, raw signal (intensity vs. time) was first smoothed (boxcar averaging) in a rolling search window. Then, the algorithm searched for a maximum intensity and the corresponding immediate minima, pre- and post-inflexion points to determine the peak width. The smoothed data preceding the pre-inflexion point was used to determine the average local background. Peak detection was triggered by a user-defined (optimized) value of intensity (not necessarily a multiple of the standard deviation of the background³¹), which was added to the average smoothed local background. The background subtracted raw data between inflexion points was integrated if the peak maximum was higher than the trigger value and the peak width larger than a set minimum (also user defined, at least 3× the dwell time and optimized depending on the dataset). Peak search then continued in a new search window, the start of which depended on whether a peak was found or not in the preceding window. For each identified peak, a full width at half maximum (FWHM) was determined and used for data filtering. For instance, peaks for which FWHM could not be calculated were identified as suspicious and manually checked for false positivity. Additionally, very large FWHM (*e.g.*, over 3× the average peak width)- indicating completely overlapping peaks- or a too noisy background were also inspected for low peak intensities. Finally, even partially overlapping peaks could be integrated using the above method, significantly increasing the accuracy of nanoparticle peak detection and integration, especially when compared to the fixed search window methods.

3. Results and discussion

3.1 Comparison of SP-ICP-SF-MS and SP-ICP-ToF-MS data

TSPP eluates from the different solid phases (Table 1) were first analyzed by SP-ICP-ToF-MS by considering a minimum threshold of 100 particles per minute (flow rate of ~0.3 mL min⁻¹). Based upon those criteria, Mg-, Al-, Si-, Ca-, Ti-, Fe-, and Ba were identified as the major elements in the CP (Fig. 1 and S2). Other CP containing Ce, Cr, K or multielement particles containing Si and K or Fe and Ce were also observed, but for a lower number of occurrences. Note that in this paper, when NP and CP are used with the symbol of a metal (*e.g.* Al-CP), it is to indicate that the element was a major constituent of the particle and not that the particle was composed solely of this element.

Although SP-ICP-ToF-MS has a valuable multielement capability, it has relatively high detection limits, leading to a higher particle size detection threshold and an inability to detect the



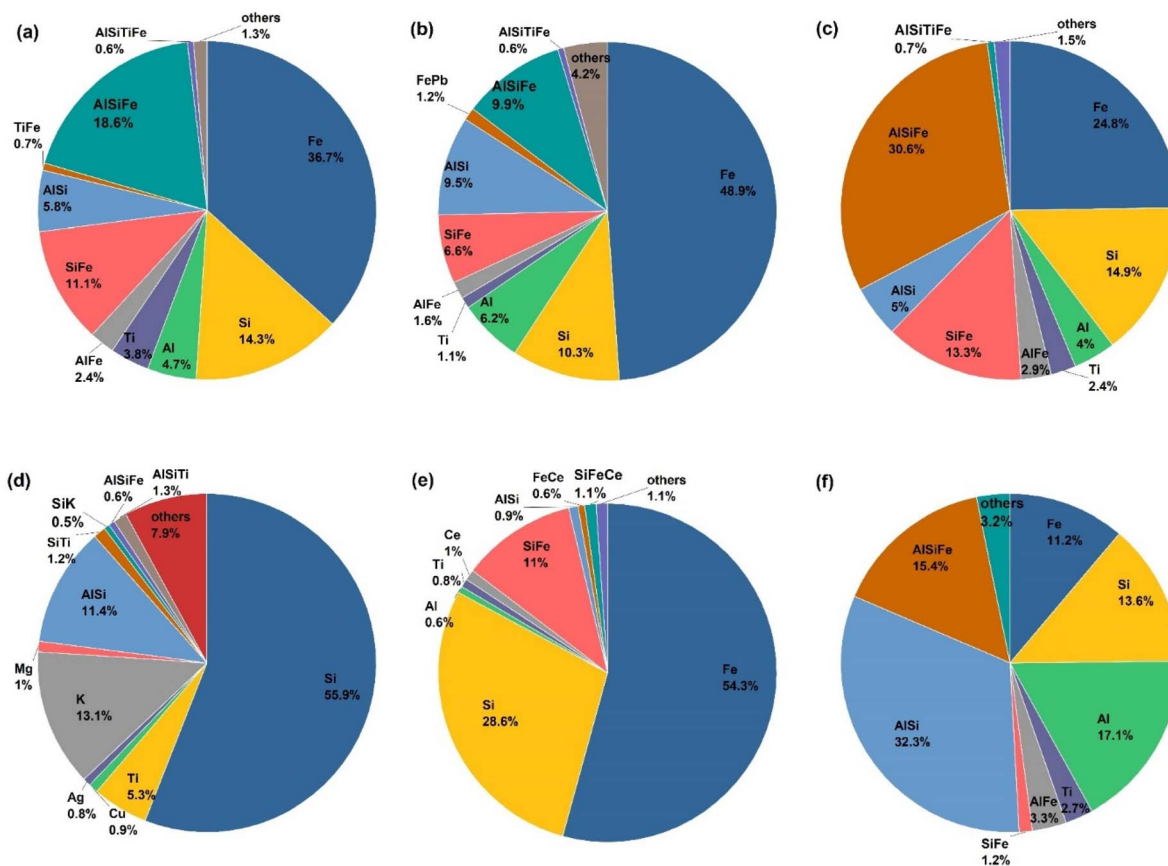


Fig. 1 Number proportion of colloidal particles detected by SP-ICP-ToF-MS in the extracts of several solid phase samples: (a) agricultural soil AG1, (b) flood plain FP, (c) agricultural soil AG2, (d) domestic sludge DS, (e) industrial sludge IS and (f) river sediment RS. These data can also be observed in the heatmaps provided in Fig. S2.

smallest particles. Mass detection limits (MDL) for Mg, Al, Si, Ca, Ti, Fe and Ba for both the sector field and time of flight instruments are summarized in Table 2.

In order to illustrate the importance of the detection limits on the particle quantification, it is possible to consider the case

of an aluminosilicate such as $\text{Al}_2\text{Si}_2\text{O}_5(\text{OH})_4$. Based upon the calculation of a spherical equivalent diameter, size detection limits (SDL) by SP-ICP-ToF-MS were calculated to be ~ 76 nm based on the sensitivity for Al and ~ 100 nm if using the sensitivity for Si. This calculation suggests that colloidal

Table 2 Typical instrument sensitivities, mass detection limits (MDL) and particle size detection limits (SDL) for Mg, Al, Si, Ca, Ti, Fe, and Ba, as obtained for SP-ICP-SF-MS and SP-ICP-ToF-MS. Values are provided for limited dissolved elements in each sample

Analyte	Particle ^a			SP-ICP-SF-MS			SP-ICP-ToF-MS				
	Molecule	Density (g cm ⁻³)	Monitored isotope	Monitored isotope	Sensitivity (count fg ⁻¹)	MDL (ag) ^b	SDL (nm)	Monitored isotope	Sensitivity (count fg ⁻¹)	MDL (ag) ^b	SDL (nm)
Mg	MgO	3.58	²⁴ Mg	²⁴ Mg	2975.3	0.7	8.7	²⁴ Mg	2.2	175.8	53.8
Al	Al ₂ O ₃	3.99	²⁷ Al	²⁷ Al	4261.7	1.2	10.2	²⁷ Al	8.3	126.5	48.6
	Al ₂ Si ₂ O ₅ (OH) ₄	2.65					15.9				75.8
Si	Al ₂ Si ₂ O ₅ (OH) ₄	2.65	²⁸ Si	²⁸ Si	188.6	11.2	33.3	²⁸ Si	4.5	303.1	100.1
	SiO ₂	2.65					25.8				77.6
Ca	CaCO ₃	2.71	⁴⁴ Ca	⁴⁴ Ca	286.0	14.9	29.7	⁴⁴ Ca	1.4	561.1	99.6
Ti	TiO ₂	4.23	⁴⁹ Ti	⁴⁹ Ti	296.8	3.8	14.2	⁴⁸ Ti	36.8	12.2	20.9
Fe	Fe ₂ O ₃	5.24	⁵⁷ Fe	⁵⁷ Fe	112.9	183.8	45.8	⁵⁶ Fe	61.2	64.8	32.3
Ba	BaSO ₄	4.50	¹³⁷ Ba	¹³⁷ Ba	762.2	1.3	9.8	¹³⁸ Ba	100.9	2.4	12.0
	BaCO ₃	4.29					9.4				11.5

^a Common compound for estimating the size. ^b Mass detection limit of the analyte.



aluminosilicates will only be measured for diameters above ~ 100 nm. Particles in the size range of 76–100 nm would be detected as Al-CP, whereas they would not be detected at all below ~ 76 nm. Based upon a sensitivity of the SP-ICP-SF-MS for Al that was more than 500 times higher than what was obtained with SP-ICP-ToF-MS (4261.7 vs. 8.3 count/fg, Table 2), the SDL (of $\text{Al}_2\text{Si}_2\text{O}_5(\text{OH})_4$) could potentially be decreased from 76 nm to 16 nm using the sector field instrument.

In order to evaluate experimentally the role of sensitivity on particle quantification, the eluates that were analysed by SP-ICP-ToF-MS were re-analysed by SP-ICP-SF-MS. As expected, significantly more colloidal particles were detected by SP-ICP-SF-MS (Fig. 2), albeit with the measurement of a single isotope in each particle. For example, the numbers of Al-CP that were determined by SP-ICP-SF-MS were 50–2200 \times higher (depending on the sample) than what was determined by SP-ICP-ToF-MS (Fig. 2). Similar differences in particle number concentrations were found for Si, Ca, and Mg, given the improved instrumental sensitivities (40 \times , 200 \times and 1350 \times , for Si, Ca, and Mg, respectively) of the SP-ICP-SF-MS with respect to the SP-ICP-ToF-MS. Even for Ti and Ba in which there was only a $\sim 8\times$ difference in sensitivity between the two instruments, about 10 \times more particles (Ti-CP and Ba-CP) were detected by SP-ICP-SF-MS as compared to SP-ICP-ToF-MS. Iron was the lone exception, due to the fact that the more abundant ^{56}Fe was monitored by SP-ICP-ToF-MS, while the less abundant ^{57}Fe was determined by SP-ICP-SF-MS, due to the absence of a reaction cell on the SF instrument. Although the measured sensitivity was nonetheless double for SP-ICP-SF-MS (Table 2), the signal to noise ratio was about 40 \times higher for the SP-ICP-ToF-MS, leading to 3–9 \times more Fe-CP detected in the different leachates by SP-ICP-ToF-MS (Fig. 2).

Similarly, with the exception of Fe, the mass distributions were significantly smaller when measured by SP-ICP-SF-MS as compared to SP-ICP-ToF-MS (Fig. S3). This point was illustrated by calculating the measured equivalent spherical diameters of the Al-containing CP under the assumption that they were

$\text{Al}_2\text{Si}_2\text{O}_5(\text{OH})_4$. While it is quite intuitive that the smallest particles are not detected by the SP-ICP-ToF-MS (see detection limits in Fig. 3), the absence of the second population of larger particles in the SP-ICP-SF-MS data is more difficult to explain. In fact, this apparent artifact results from the stochastic nature of the SP techniques. In SP-ICP-MS, particle number concentrations (PNC) must be adjusted into a relatively small concentration window from *ca.* 100 to 2000 particles min^{-1} . Indeed, the probability of particle coincidences increases at the higher PNC, whereas at the lower PNC, it is important to have sufficient particles in order to maintain statistical relevance. As seen above for Al CP, there were between 50 and 2200 \times more particles in the smaller size fraction (SP-ICP-SF-MS) than in the

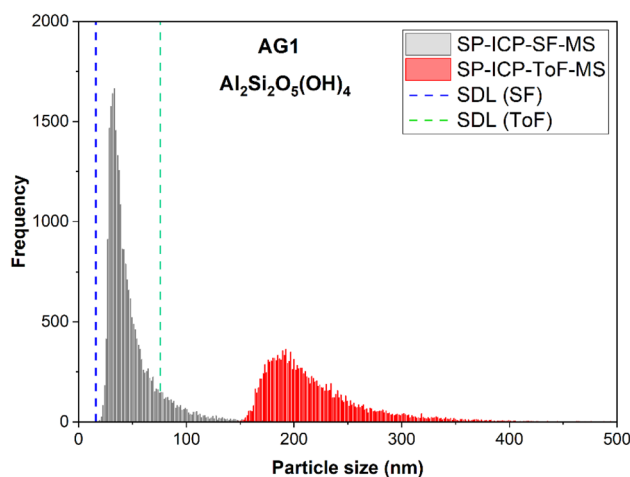


Fig. 3 Particle size distribution of a CP assumed to be an aluminosilicate ($\text{Al}_2\text{Si}_2\text{O}_5(\text{OH})_4$). Sizes are determined from the mass of Al-containing CP extracted from agricultural soil (AG1) and measured by SP-ICP-SF-MS and SP-ICP-ToF-MS. In this figure, the sizes of the peaks have been adjusted to reflect the different sample dilutions used for analysis (10 \times greater dilution for SP-ICP-SF-MS with respect to SP-ICP-ToF-MS). Accumulation time was 6 minutes for SP-ICP-SF-MS and 18 minutes for SP-ICP-ToF-MS.

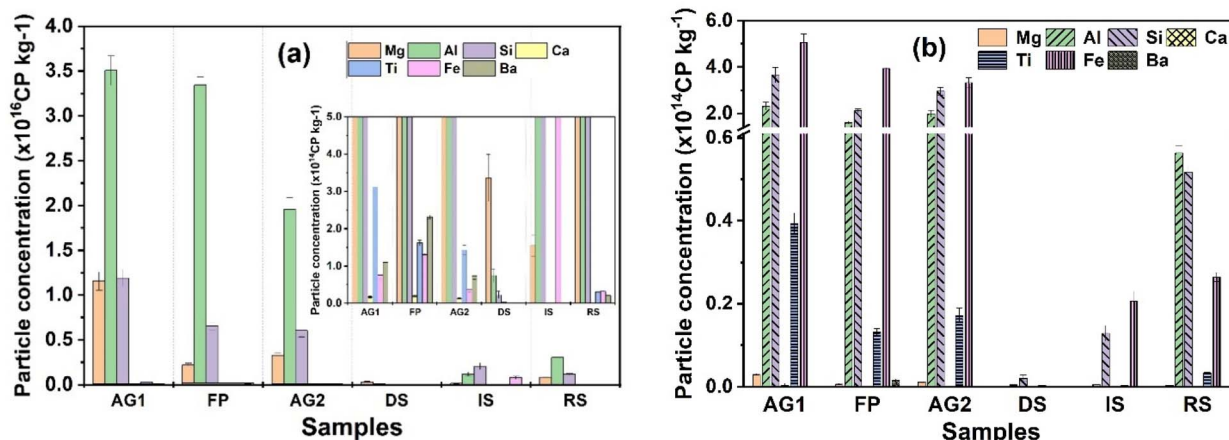


Fig. 2 Number concentrations of Mg-, Al-, Si-, Ca-, Ti-, Fe-, and Ba-CP extracted from agricultural soils (AG1 and AG2), a flood plain soil (FP), a domestic sludge (DS), an industrial sludge (IS) and a river sediment (RS). Data are acquired using (a) SP-ICP-SF-MS and (b) SP-ICP-ToF-MS. The inset in (a) uses a 100 \times increase in scale to better see the results of the lower frequency elements.



fraction measured by SP-ICP-ToF-MS. By adjusting the concentration of the smallest particles to 2000 particles per min, one necessarily reduces the number of larger particles to a few spikes on the chromatogram, concentrations that are likely to be below statistical relevance. The limits and capabilities of SP-ICP-SF-MS and SP-ICP-ToF-MS are examined further for two aluminosilicates: $\text{Al}_2\text{Si}_2\text{O}_5(\text{OH})_4$ and $\text{Fe}_3\text{Al}_2(\text{SiO}_4)_3$ in Fig. S4, where it is shown schematically how only a fraction of the particles can be detected at a given dilution. Given the above observations, it is critical to use multiple SP-ICP-MS techniques in order to extend observations across particle size ranges, in addition to performing measurements at multiple dilutions.³² The combination of multiple data sources is very important for getting better insight into the analysis of chemically complex and polydisperse systems, such as soil CP and NP. In addition, it is important to be extremely careful/critical when interpreting SP-ICP-ToF-MS data. Given the above caveats, in the discussion that follows, SP-ICP-SF-MS was mainly used to compare particle numbers of the smaller CP and NP, while SP-ICP-ToF-MS was primarily used to characterize the multi-elemental or multi-isotopic composition of the particles.

3.2 Characterization of the solid phase colloidal particles by SP-ICP-SF-MS

The highest numbers of extracted particles were found in the leachates from the agricultural and flood plain soils (AG1, AG2, and FP), with Al-CP representing the largest proportion of the particles (Fig. 2a). For identical extraction conditions, about ten times fewer particles were extracted from the industrial sludge (IS) and the river sediment (RS), with the domestic sludge (DS) having even lower numbers of extractable and measurable colloidal particles. In all cases, Mg-, Al-, and Si-CP were the most abundant particles in the leachates, consistent with the presence of aluminosilicates. Furthermore, in spite of the common use of titanium dioxide in domestic products and pharmaceuticals, very few Ti-CP were found in either the domestic or industrial sludges (*ca.* 0.04% and 0.12% of the total titanium, respectively (Table 3)). This low proportion of Ti-CP may result from several potential mechanisms: (i) their strong interactions with solid matter may lead to the formation of large (micro- or macro-sized) aggregates, which could not be extracted or measured by ICP-MS; (ii) decreased transport in the ICP-MS due

to sedimentation losses could occur during the sample introduction, including nebulization; or (iii) poorer ionization or decreased transport efficiency may be decreasing detection of the larger particles.³³ With a few exceptions such as the measurement of relatively larger Mg-CP and Al-CP in the domestic sludge, the mass (hence the size) distributions of extracted CP were very similar (Fig. S3). This observation may have resulted from the combined use of TSPP²⁷ and ultrasound during the extraction process, which could lead to a reduced particle polydispersity.

3.3 Elemental molar ratios of single particles by ICP-ToF-MS

Elemental molar ratios are one indicator that can be used to distinguish among the different colloidal solid phases. For example, binary Al/Fe ratios showed clear differences among the different samples (Fig. 4). Contrary to elemental molar ratios performed on the bulk sample, the elemental molar ratios presented here are a histogram of ratios obtained for individual particles, implying that the breadth of the distribution is a good indicator of the chemical heterogeneity of the samples. In that light, the two agricultural soils (Fig. 4a and c) had broad distributions with relatively large values Al/Fe ratios. In contrast, the industrial sludge (Fig. 4e) had a narrow distribution of extremely low Al/Fe values.

Furthermore, given the wealth of information obtained from ICP-ToF-MS, ternary diagrams are another effective means for distinguishing among the solid phase samples. For example, in Fig. 5, single particle ICP-ToF-MS measurements provide a distribution of Al:Fe:Si ratios (blue points) that take into account the chemical heterogeneity of the sample, whereas, bulk measurements provide an average value only ('half full red circle' in Fig. 5, as determined from the certified values). Clearly, the Al:Fe:Si ratios are fairly widely dispersed and/or show multiple populations of the particles (*e.g.*, Fig. 5a and b). Furthermore, by comparing the measured elemental ratios with those of pure mineral phases, it is possible to speculate on the probable, predominant types of minerals within the solids. For example, for the agricultural and flood plain soils, the majority of the colloidal particles containing Al, Si and Fe were found with molar proportions of 12–50% Al, 50–85% Si and 5–13% Fe. These values are consistent to values that would be seen with illite, vermiculite or smectite mineral phases. In contrast,

Table 3 Measured mass fraction (%) of extracted colloidal Mg, Al, Si, Ca, Ti, Fe and Ba relative to the certified proportions in the solid samples. The relatively low values result from both the extraction (not all particles are extracted from a soil) and from the measurement (ICP-MS has an upper limit on particle sizes that can be efficiently nebulized and ionized). CP were extracted from the different solid phase samples (AG1, AG2, FP, DS, IS and RS) using ultrasound assisted extraction with 40 mM TSPP (pH = 6.0) and analyzed by SP-ICP-SF-MS

	AG1	FP	AG2	DS	IS	RS
Mg	2.40 ± 0.15	1.17 ± 0.16	1.46 ± 0.14	1.09 ± 0.23	0.696 ± 0.175	0.332 ± 0.071
Al	1.45 ± 0.10	1.27 ± 0.05	1.04 ± 0.11	0.022 ± 0.007	0.088 ± 0.019	0.286 ± 0.028
Si	1.26 ± 0.13	0.609 ± 0.055	0.746 ± 0.128	0.030 ± 0.009	0.182 ± 0.028	NA
Ca	0.023 ± 0.004	0.040 ± 0.003	0.015 ± 0.002	0.003 ± 0.001	0.005 ± 0.001	0.005 ± 0
Ti	1.91 ± 0.19	0.675 ± 0.075	0.826 ± 0.069	0.038 ± 0.012	0.119 ± 0.023	0.221 ± 0.007
Fe	0.842 ± 0.151	1.38 ± 0.01	0.432 ± 0.068	0.014 ± 0.003	0.922 ± 0.181	0.322 ± 0.001
Ba	0.365 ± 0.036	1.35 ± 0.05	0.247 ± 0.033	NA	0.007 ± 0.001	0.244 ± 0.011



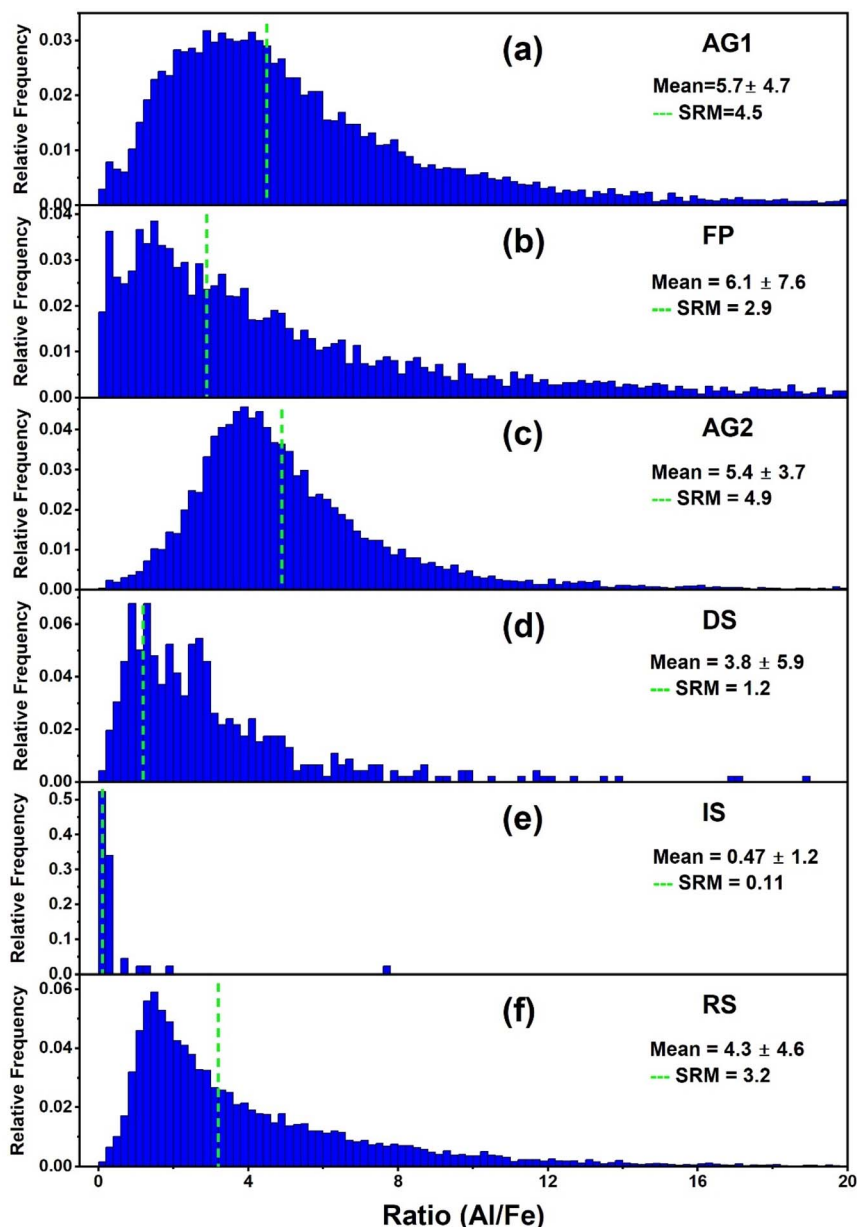


Fig. 4 Al/Fe molar ratios in the individual particles extracted from the different solid samples ((a) AG1, (b) FP, (c) AG2, (d) DS, (e) IS and (f) RS) as measured by SP-ICP-ToF-MS. The bulk value of the molar ratio, as obtained from the published concentrations of the SRM, are presented as the vertical green dashed line. Means and standard deviations are presented in the figure.

for the industrial sludge, there were few detected particles containing these three elements; Si:Fe molar ratios (mean value of 0.58 ± 0.98 , $n = 2787$ CP) are similar to those of fayalite.

3.4 Isotopic ratios of single particles by ICP-ToF-MS

Isotopic ratios of the individual particles were also evaluated with the hypothesis that some isotopic enrichment could be observed for particles derived from specific (likely industrial) events.^{34–38} Nonetheless, the accuracy of isotopic ratios measured at a single particle level (*i.e.* very short transient signal) appears to be highly impacted by the particle size and instrument sensitivity. Indeed, as reported in the literature,^{39–41}

and based upon the measurements carried out in this study, extremely high variability was observed for the smallest particles (Fig. 6c and S5). This high uncertainty can be attributed to the stochastic nature of ion detection at low ion counts.⁴² Furthermore, the measurement of the larger particles can, in some cases, be inaccurate due to detector saturation or reduced transport efficiency. This high uncertainty makes it difficult to quantify the typically small effects of isotopic fractionation that may be occurring as a result of environmental processes, such as chemical sorption/complexation.⁴³

In addition to the uncertainties inherent with the measurements of isotopic ratios, some systematic errors are possible due to instrumental mass bias. Based upon the isotopic ratios



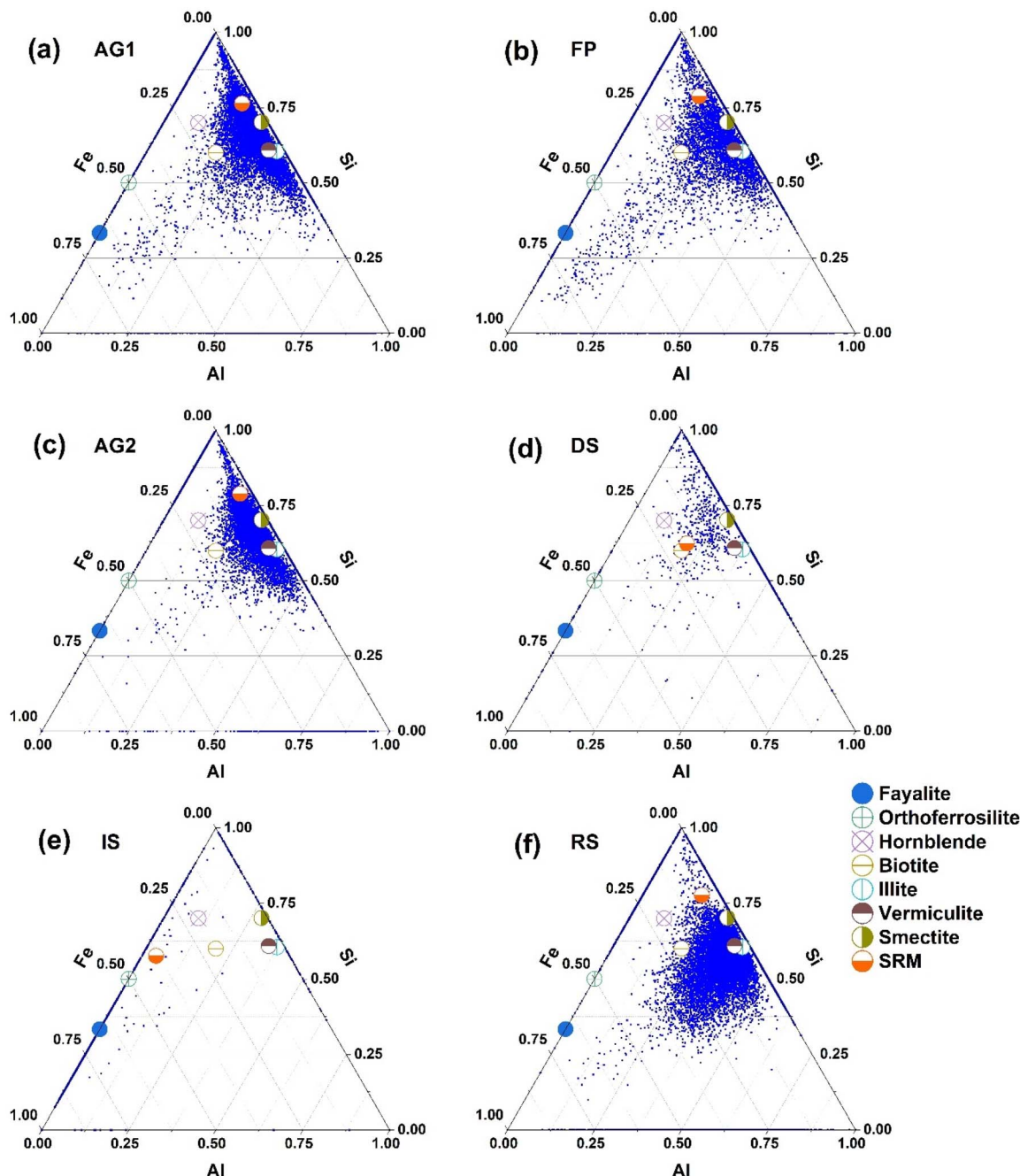


Fig. 5 Molar proportions of Al-, Si- and Fe- in CP extracted from different solid samples: (a) AG1, (b) FP, (c) AG2, (d) DS, (e) IS and (f) RS as analyzed by SP ICP-ToF-MS. Values for the SRM are calculated from its certified values. Values for the mineral phases were calculated from their chemical formulae.

in the ionic standards, a correction to the mass bias was performed, however, there was still a positive shift of the average of isotopic ratios of particles with respect to natural isotopic ratios for all measured isotopes (Fig. S5). It is difficult to attribute this shift to actual isotopic fractionation or to an additional mass bias due to the measurement of the fast transient signal. Therefore, additional SP-ICP-ToF-MS measurements were carried out using a certified reference materials for lead isotopes (NIST SRM 981), which was solubilized and analyzed at

different concentrations (from 5 to 9 $\mu\text{g L}^{-1}$), along with the leachates under the same conditions. A correction factor for mass bias (CF_{mb}) was defined as the measured over certified isotopic ratio $^{206}\text{Pb}/^{207}\text{Pb}$ for the SRM 981 and ionic standards (eqn (S1)). It was plotted as a function of ^{207}Pb intensity, which was measured for different concentrations of the ionic Pb standard (Fig. 6a). From the relationship between CF_{mb} and ^{207}Pb intensity, a polynomial fit (eqn (S2)) could be generated (eqn (S2)), which could be used to correct the mass bias of the



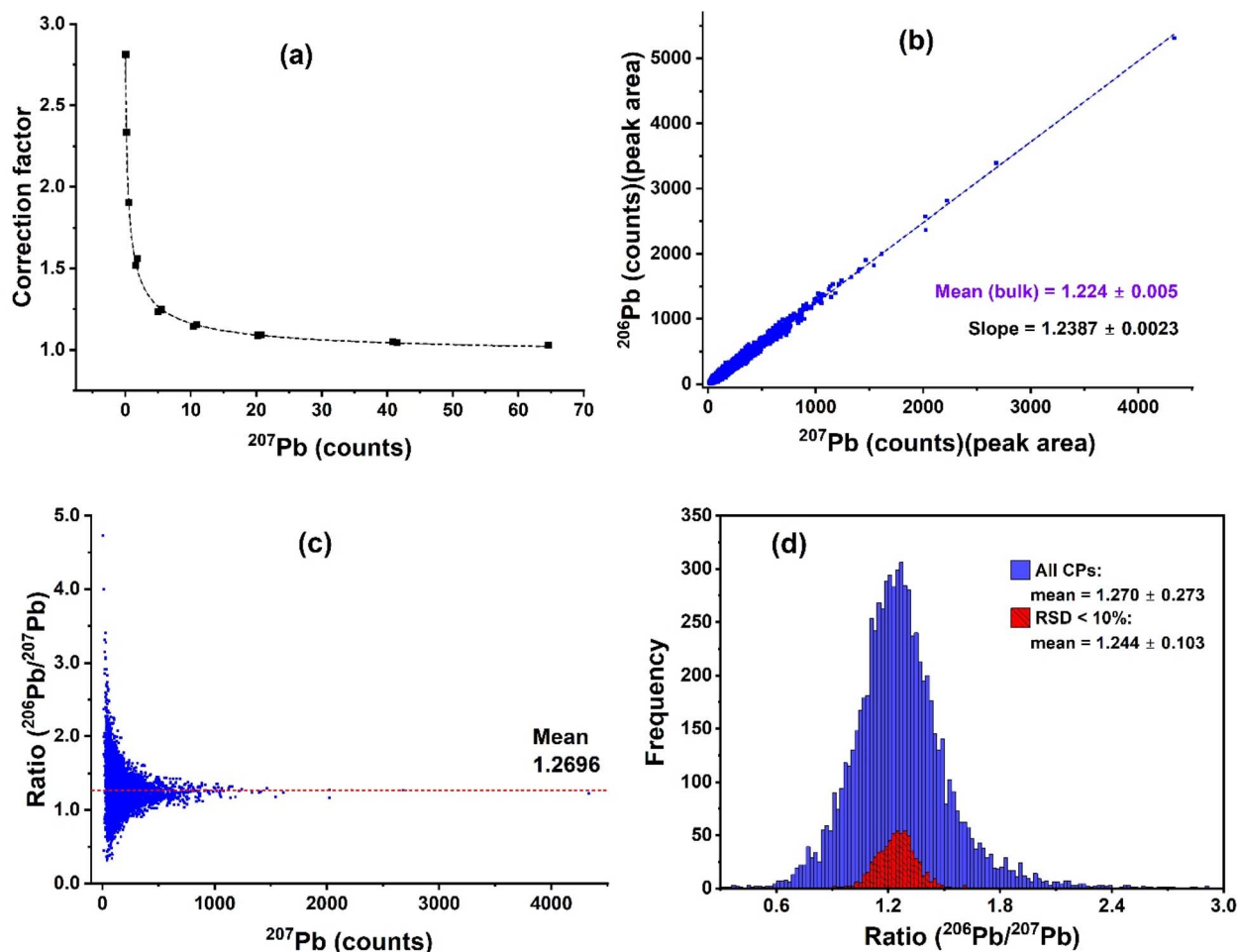


Fig. 6 (a) Correction factor for mass bias as a function of ^{207}Pb intensity in NIST SRM 981, as measured by the SP-ICP-ToF-MS. (b) Isotopic plot of ^{206}Pb vs. ^{207}Pb for the leachate of the flood plain sample (FP); (c) isotopic ratio of $^{206}\text{Pb}/^{207}\text{Pb}$ as a function of the ^{207}Pb intensity (i.e. particle size) for the leachate of the flood plain sample (FP) and (d) distribution of isotopic ratio $^{206}\text{Pb}/^{207}\text{Pb}$ for the leachate of the flood plain sample (FP). In (b), standard deviations are determined from either triplicate measurements of the digested solution (bulk) or from the error on the slope (single particle measurements). In (d), single particle measurements were again used to determine isotope ratios, however, standard deviations were determined from either the full distribution of values (shown in (c)) or filtered to remove values that were furthest from the mean (corresponding to the smallest ^{207}Pb measurements and shown in Fig. S8) for the small distribution (red).

measured intensity of ^{206}Pb in individual particles extracted from the different solid samples (Fig. 6a and S6). The corrected values were plotted (Fig. 6b and c) to obtain the $^{206}\text{Pb}/^{207}\text{Pb}$ isotopic ratios. Fig. 6d shows the distribution of isotopic ratios for data in which the very small particles (based upon a relative standard deviation of 10%, Fig. S8) were eliminated from the dataset. Finally, aliquots of the extracts were also digested and analyzed for bulk isotopic ratios using a longer dwell time of 130 ms. The results are reported in Table 4 in which the relative differences between isotopic ratios in the bulk and single particles were determined. Deviations from the natural abundance ratios were also evaluated.

With respect to the bulk ratios determined on the digested extracts, a substantial enrichment (from 10.31 to 18.35%) of ^{206}Pb , relative to ^{207}Pb , was observed for all samples except for the agricultural soil AG2 (smaller deviation of 0.34%). Note however that for each extract, a non negligible relative

difference (1.20–5.92%) was found between the isotopic ratio in the bulk extract with respect to that in the individual particles. On the one hand, the ratios in the digested extracts involved both dissolved and particulate Pb. On the other hand, particles detected by SP-ICP-ToF-MS represent only a fraction of all extracted particles, which may not be representative of the nano or colloidal phases of the sample. Thus, it is likely that both approaches are measuring isotopic ratios in different populations of Pb atoms. Nonetheless, while it will be necessary to examine more deeply this discrepancy, it is clear that the determination of isotopic ratios on individual colloidal particles will be of great interest to the scientific community. Finally, it is important to acknowledge that for an in-depth investigation of isotopic ratios of other elements, it will be key to use SRMs of nanoparticles with certified isotopic ratios (once available) in order to validate the use of SP-ICP-ToF-MS for isotopic ratio determinations.



Table 4 Isotopic ratios of $^{206}\text{Pb}/^{207}\text{Pb}$ for bulk digested extracts compared with linear correlated ratios of individual colloidal particles (CP), extracted from different solid samples. Relative differences (final two columns) are calculated as $100 \times |A - B|/B$, where A is the isotopic ratio of the digested sample and B is the accepted natural ratio obtained from NIST SRM 981 (1.0933) (column 6) or A is the isotopic ratio determined on the single particles (CP) and B is the ratio for the digested sample (column 7)

Sample	Bulk digested extract	Colloidal particles				Relative difference (%)	
		Linear correlation		Particle number	Bulk Natural	CP Bulk	
		Slope	R^2				
AG1	1.26 ± 0.045	1.312	0.9714	660	15.24	4.13	
FP	1.224 ± 0.005	1.239	0.9743	7520	11.95	1.23	
AG2	1.097 ± 0.001	1.162	0.9805	619	0.34	5.93	
DS	1.294 ± 0.017	1.339	0.9919	348	18.35	3.48	
IS	1.249 ± 0.004	1.295	0.9801	107	14.24	3.68	
RS	1.206 ± 0.001	1.266	0.9888	183	10.31	4.98	

4. Conclusion

When examining chemically heterogeneous and polydisperse samples such as soils, sediments and sludges, the single particle techniques, including SP-ICP-SF-MS and SP-ICP-ToF-MS, are able to provide unique information that is not available through bulk measurements. Indeed, bulk analysis of the solid phases examined here showed few differences among the samples, whereas clear and important differences were observed for trace element distributions and elemental ratio distributions (binary and ternary) when measuring the single particles. Nonetheless, further work will be required when measuring the isotope ratios of individual colloidal particles in order to determine to what extent further improvements in accuracy and precision can be made, especially when attempting to distinguish between relatively small differences in samples. Furthermore, when determining particle number concentrations and particle size distributions, great care will be required due to the relatively limited dynamic range of these techniques. The use of multiple techniques is one way to get a more complete picture of a complex sample, however, as was shown, the two SP-ICP-MS techniques used here gave complementary but different particle size distributions. Future work will be necessary but useful to further exploit the potential of the single particle techniques to thoroughly characterize complex samples.

Author contributions

Zhizhong Li developed and conducted the experiments, treated acquired data and arranged the data into figures and tables, as well as preparing the first draft of the paper. Madjid Hadioui was involved with the preparation and interpretation of all ICP-SF-MS and ICP-ToF-MS experiments and assisting with the paper drafts. Kevin Wilkinson provided resources and practical suggestions for the experiments and contributed to data interpretation and all drafts of the paper.

Conflicts of interest

There are no conflicts to declare.

Data availability

Much of the data supporting this article is included as part of the SI. All raw data, in the form of CSV files, and metadata are available at [10.5281/zenodo.16737786](https://doi.org/10.5281/zenodo.16737786).

Experimental setup, elemental heatmaps of samples, mass distributions, isotope ratio calculations and examples. See DOI: <https://doi.org/10.1039/d5ja00181a>.

Acknowledgements

We acknowledge the financial support of the NSERC Discovery in addition to the Fonds de recherche du Québec – Nature et technologies. Helpful insights gained during discussions with Houssame-Eddine Ahabchane and Aaron Goodman are greatly appreciated.

References

- J. R. Lead and K. J. Wilkinson, in *Environmental Colloids and Particles*, 2006, pp. 1–15, DOI: [10.1002/9780470024539.ch1](https://doi.org/10.1002/9780470024539.ch1).
- L. N. Du, C. W. Cuss, M. Dyck, T. Noernberg and W. Shotyk, *Sci. Total Environ.*, 2024, **924**, 171590.
- H. El Hadri, J. Gigault, P. Chéry, M. Potin-Gautier and G. Lespes, *Anal. Bioanal. Chem.*, 2014, **406**, 1639–1649.
- C. Y. Xu, T. T. Zhou, C. L. Wang, H. Y. Liu, C. T. Zhang, F. N. Hu, S. W. Zhao and Z. C. Geng, *Geoderma*, 2020, **359**, 113999.
- M. D. Montaña, B. J. Majestic, Å. Jämting, P. Westerhoff and J. F. Ranville, *Anal. Chem.*, 2016, **88**, 4733–4741.
- E. Bolea-Fernandez, D. Leite, A. Rua-Ibarz, L. Balcaen, M. Aramendía, M. Resano and F. Vanhaecke, *J. Anal. Atom. Spectrom.*, 2017, **32**, 2140–2152.
- Y. P. Gao, Y. Yang, L. Li, W. J. Wei, H. Xu, Q. Wang and Y. Q. Qiu, *Anal. Chim. Acta*, 2020, **1110**, 72–81.
- A. Azimzada, I. Jreije, M. Hadioui, P. Shaw, J. M. Farner and K. J. Wilkinson, *Environ. Sci. Technol.*, 2021, **55**, 9836–9844.
- W. Y. Liu, H. L. Shi, K. Liu, X. S. Liu, E. Sahle-Demessie and C. Stephan, *J. Agric. Food Chem.*, 2021, **69**, 1115–1122.
- T. Hirata, S. Yamashita, T. Suzuki and M. Ishida, *Bunseki Kagaku*, 2019, **68**, 81–88.



- 11 S. Yamashita, K. Yamamoto, H. Takahashi and T. Hirata, *J. Anal. Atom. Spectrom.*, 2022, **37**, 178–184.
- 12 P. J. Xing, N. S. Belshaw, J. H. Dong, L. J. Li, Y. H. Geng, H. T. Zheng, X. Liu and Z. L. Zhu, *Talanta*, 2024, **278**, 126540.
- 13 M. A. Millet and N. Dauphas, *J. Anal. Atom. Spectrom.*, 2014, **29**, 1444–1458.
- 14 B. T. Manard, V. C. Bradley, C. D. Quarles, Jr, L. Hendriks, D. R. Dunlap, C. R. Hexel, P. Sullivan and H. B. Andrews, *Nanomaterials*, 2023, **13**, 1322.
- 15 Z. W. Meng, L. N. Zheng, H. Fang, P. Yang, B. Wang, L. Li, M. Wang and W. Y. Feng, *Processes*, 2023, **11**, 1237.
- 16 G. D. Bland, M. Battifarano, A. E. P. del Real, G. Sarret and G. V. Lowry, *Environ. Sci. Technol.*, 2022, **56**, 2990–3001.
- 17 S. E. Szakas, R. Lancaster, R. Kaegi and A. Gundlach-Graham, *Environ. Sci. Nano*, 2022, **9**, 1627–1638.
- 18 S. E. Szakas and A. Gundlach-Graham, *J. Anal. Atom. Spectrom.*, 2024, **39**, 1874–1884.
- 19 J. J. Wang, M. M. Nabi, M. Erfani, E. Goharian and M. Baalousha, *Environ. Sci. Nano*, 2022, **9**, 714–729.
- 20 F. Wang, M. Tharaud and M. F. Benedetti, *Microchem. J.*, 2024, **203**, 110843.
- 21 I. C. Regelink, L. Weng, G. F. Koopmans and W. H. Van Riemsdijk, *Geoderma*, 2013, **202**, 134–141.
- 22 S. Baur, T. Reemtsma, H. J. Stärk and S. Wagner, *Chemosphere*, 2020, **246**, 125765.
- 23 W. Li, Y. He, J. Wu and J. Xu, *Eur. J. Soil Sci.*, 2012, **63**, 754–761.
- 24 F. Loosli, Z. B. Yi, J. J. Wang and M. Baalousha, *Sci. Total Environ.*, 2019, **677**, 34–46.
- 25 Z. Li, M. Hadioui and K. J. Wilkinson, *Nanomaterials*, 2023, **13**, 2049.
- 26 D. M. Schwertfeger, J. R. Velicogna, A. H. Jesmer, S. Saatcioglu, H. McShane, R. P. Scroggins and J. I. Princz, *Anal. Chem.*, 2017, **89**, 2505–2513.
- 27 Z. Li, M. Hadioui and K. J. Wilkinson, *Nanomaterials*, 2023, **13**, 2049.
- 28 A. Azimzada, J. M. Farner, I. Jreije, M. Hadioui, C. Liu-Kang, N. Tufenkji, P. Shaw and K. J. Wilkinson, *Front. Environ. Sci.*, 2020, **8**, 2020.
- 29 P. Shaw and A. Donard, *J. Anal. Atom. Spectrom.*, 2016, **31**, 1234–1242.
- 30 K. Newman, C. Metcalfe, J. Martin, H. Hintelmann, P. Shaw and A. Donard, *J. Anal. Atom. Spectrom.*, 2016, **31**, 2069–2077.
- 31 M. Hadioui, G. Knapp, A. Azimzada, I. Jreije, L. Frechette-Viens and K. J. Wilkinson, *Anal. Chem.*, 2019, **91**, 13275–13284.
- 32 S. G. Bevers, C. Smith, S. Brown, N. Malone, D. H. Fairbrother, A. J. Goodman and J. F. Ranville, *Environ. Sci. Nano*, 2023, **10**, 3136–3148.
- 33 M. Lomax-Vogt, L. M. Carter, J. Wielinski, S. Kutuzov, G. V. Lowry, R. Sullivan, P. Gabrielli and J. W. Olesik, *J. Anal. Atom. Spectrom.*, 2025, **40**, 848–859.
- 34 D. Lu, Q. Liu, M. Yu, X. Yang, Q. Fu, X. Zhang, Y. Mu and G. Jiang, *Environ. Sci. Technol.*, 2018, **52**, 1088–1095.
- 35 M. Mercurio, P. Cappelletti, V. Di Renzo, C. Grifa, C. Guarino, F. Izzo, P. Magliulo, V. Mercurio, P. Tranfa, D. Zuzolo, M. D'Antonio and A. Langella, *Data Brief*, 2024, **55**, 110686.
- 36 A. Vanek, T. Dordevic, M. Mihaljevic, M. Vankova, K. Fizkova, T. Zadorova, P. Vokurkova, I. Galuskova, V. Penizek, O. Drabek, G. Tasev, T. Serafimovski, I. Boev and B. Boev, *Environ. Pollut.*, 2024, **357**, 124413.
- 37 A. Wahl, M. Davranche, A. Dia, D. Vilbert, I. Khatib, M. Pattier, N. Ryzhenko, M. B. Coz, G. Peres, C. Catrouillet, A. C. Pierson-Wickmann and J. Gigault, *J. Hazard. Mater.*, 2024, **476**, 135153.
- 38 Z. A. Alqattan, A. Trahan, G. N. Chukwuonye, M. Jones and M. D. Ramirez-Andreotta, *Environ. Res.*, 2025, **271**, 121130.
- 39 K. H. Chun, J. T. Lum and K. S. Leung, *Anal. Chim. Acta*, 2022, **1192**, 339389.
- 40 B. T. Manard, V. C. Bradley, C. D. Quarles, L. Hendriks, D. R. Dunlap, C. R. Hexel, P. Sullivan and H. B. Andrews, *Nanomaterials*, 2023, **13**, 1322.
- 41 S. Yamashita, M. Ishida, T. Suzuki, M. Nakazato and T. Hirata, *Spectrochim. Acta B*, 2020, **169**, 105881.
- 42 M. Nakazato and T. Hirata, *Anal. Sci.*, 2025, **41**, 1185–1201.
- 43 M. Komárek, G. Ratić, Z. Vaňková, A. Šípková and V. Chrástný, *Crit. Rev. Environ. Sci. Technol.*, 2021, **52**, 3573–3603.

